JOURNAL OF MATERIALS SCIENCE 22 (1987) 381–393

Review
Parameters determining the strength and toughness of particulate filled epoxide resins

A. C. MOLONEY, H. H. KAUSCH
Laboratoire de Polymères, Ecole Polytechnique Fédérale de Lausanne, 32, ch. de Bellerive, 1007 Lausanne, Switzerland

T. KAISER, H. R. BEER
Zentrallabor, Ress. Kunststoffe und Keramik, Brown Boveri & Cie. AG., Affolternstrasse 52, 8050 Zürich-Oerlikon, Switzerland

The effects of such parameters as the filler volume fraction, particle size, aspect ratio, modulus and strength of filler, resin–filler adhesion and toughness of the matrix on the stiffness, strength and toughness of particulate filled epoxide resins have been evaluated. The mechanisms of deformation and rupture in these multiphase materials are discussed, illustrated by *in situ* mechanical tests in the scanning electron microscope.

1. Introduction

The mechanical behaviour of particulate filled epoxide resins results from a complex interplay of the properties of the constituent phases: resin, filler and interfacial region. The principal relevant parameters are the volume fraction of filler, the particle size, the filler aspect ratio, the modulus and strength of the filler, the resin–filler adhesion and the toughness of the matrix. The variation of certain of these parameters leads to improved toughness of the filled material, however, this may be to the detriment of the strength and modulus. The objective of this paper is to discuss the influence of the above parameters on the strength, stiffness and toughness of the resulting composite.

It must be noted that two other properties are of considerable importance in the processing and application of these materials. Firstly, the viscosity of the uncured mixture must be sufficiently low to permit the evacuation of air bubbles. Secondly, for many uses the glass transition temperature is critical. For example in high and medium voltage insulators the filled material must have a glass transition temperature of at least 120° C in order to withstand the temperatures attained around the electrode. Thus, these two requirements will restrict the unlimited variation of the above parameters.

2. Volume fraction of filler

Epoxide resins in the uncured state have relatively high viscosities as compared with polyesters, for example. Thus for most practical systems the maximum volume fraction of filler which may be incorporated is ~50% to avoid the presence of voids. At low volume fractions (up to 30%) sedimentation occurs. In order to produce homogeneous castings either the moulds must be rotated [1] or else the mixture must be poured just prior to gelation [2].

The effect of increasing the volume fraction of filler on the modulus of the composite is now well documented in the literature for a wide range of epoxide resins and filler materials [3–6]. Fig. 1 shows the general parabolic relationship which has been found between these two parameters. For epoxide resins possessing high glass transition temperatures crack propagation is, in general, stable when particulate fillers are incorporated. For this type of system there exists a linear relationship between the stress intensity factor and the filler volume fraction as shown in Fig. 2. This same type of relationship has been observed for a number of brittle unmodified epoxide resins. Increasing the volume fraction of the filler gives a composite with tensile strength at best equal to that of the unfilled matrix. This is shown in Table I for a brittle epoxide resin filled with silica particles. At 20% volume fraction the tensile strength is lower than that of the matrix and then there is a steady increase until at 50% the matrix value of 78 MPa is achieved. A similar result was obtained by Spandoukis and Young [7] for another epoxide resin filled with silane treated glass beads (see Fig. 3).

Thus we may conclude that increasing filler volume fraction increases the modulus and toughness and can give castings with strength comparable to the matrix.

TABLE I Mechanical properties of a silica filled resin as a function of volume fraction

Volume fraction (%)	Tensile strength (MPa)	Tensile modulus (GPa)	Flexural strength (MPa)	Flexural modulus (GPa)	Compressive yield stress (MPa)
0	78.5	3.4	–	–	98.4
20	47.1	6.6	90.2	6.9	129.0
40	63.9	12.2	98.3	12.2	154.0
50	78.0	18.5	108.1	17.6	–

0022–2461/87 $03.00 + .12

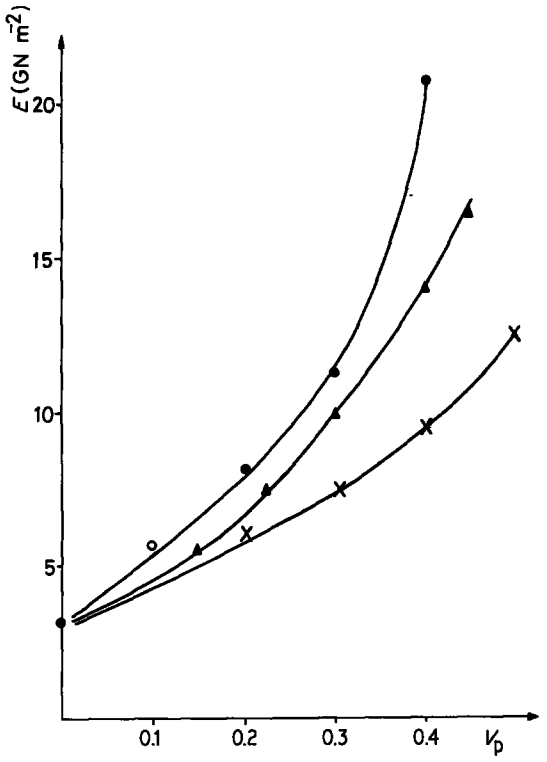

Figure 1 Flexural modulus, E, as a function of volume fraction of filler: x, silica; ▲, alumina; ●, silicon carbide.

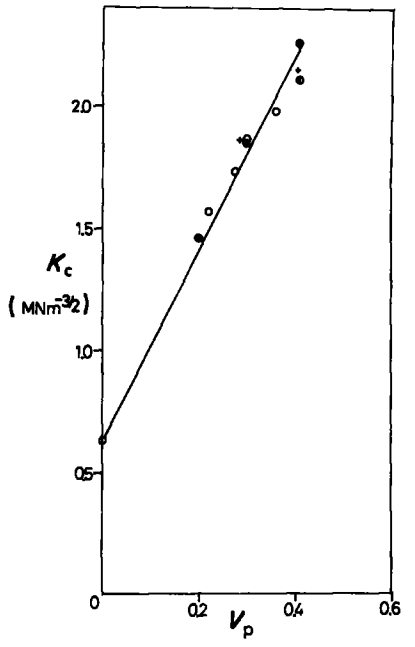

Figure 2 Stress intensity factor as a function of volume fraction of filler. ○, Al_2O_3; ●, SiO_2; ◐, silane treated SiO_2.

3. Filler particle size

Changing the filler particle size at constant volume fraction does not have a significant influence on the modulus of the composite. Spandoukis and Young [7, 8] have used glass beads of 4.5 and 62 μm in diameter. The modulus of the composite with 4.5 μm particles was slightly higher but in fact just outside the scatter band of the data (see Fig. 4). Similarly our own experiments on silica filled resin showed that varying the mean particle size between 60 and 300 μm did not appreciably alter either the modulus or the stress intensity factor at constant volume fraction (Table II). For the range of particle sizes investigated by Spandoukis and Young there was no difference in the strength of the castings at constant volume fraction for well-bonded beads. However, it is clear that there is an upper boundary in particle size where the strength is adversely affected due to the higher probability of a flaw being present within the particle. Table II shows that the strength does indeed decrease with increasing size of silica particles. The inclusion of particles inferior in size to 4.5 μm may well improve the strength of the composite; however, a practical limit is imposed by the viscosity of the mixture. Smaller particles have a greater surface area and thus considerably increase the viscosity.

4. Modulus and strength of particles

Increasing the filler modulus increases the modulus of the resulting composite. This is clearly shown in Fig. 1 for an epoxide resin filled with silica, alumina and silicon carbide particles. The moduli of these filler materials are 94, 320 and 469 GPa, respectively. Similarly, increasing the modulus of the filler increases the stress intensity factor (K_c) as shown in Fig. 5. The K_c values of the silicon carbide composites were significantly higher than for the silica and alumina systems. In the case of dolomite filled resin [6] above 25 vol % a plateau is reached in the stress intensity factor. This

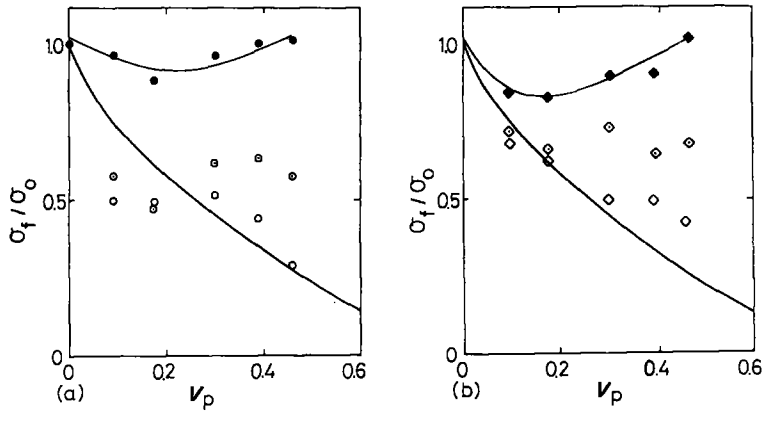

Figure 3 Ratio of the fracture stress of the composite to that of matrix σ_f/σ_0 as a function of volume fraction of filler. (a) 4.5 μm particles, ●, treated with A187; ○, DC 1107 treated; ⊙, untreated. (b) 62 μm particles, ◆, treated with A187; ◇, DC 1107 treated; ⟐, untreated (after Spandoukis and Young [7]).

TABLE II The effect of filler particle size on mechanical properties of silica filled resin (40 vol %)

Mean particle size (μm)	K_c (MPa m$^{1/2}$)	Flexural modulus (GPa)	Flexural strength (MPa)
300	1.76	10.2	60.9
160	1.74	12.1	74.5
100	1.87	10.3	79.1
60	1.85	10.0	122.7

corresponds to the onset of transparticle fracture; dolomite particles being weak compared to silica and alumina. If extremely weak particles are used (such as hollow silica microspheres of mean diameter 50 μm and a wall thickness of 1.5 μm) no toughening at all is obtained. The stress intensity factor of the composite prepared from 30% by volume of the hollow spheres was exactly the same as the epoxide matrix (0.6 MPa m$^{1/2}$). The micrograph in Fig. 6 shows clearly that cracks have propagated directly through the particles. Thus, the mere presence of interfaces does not impede crack growth as has been suggested [9]. The second phase material must have sufficient inherent toughness to be effective. It is evident that these "weak" particles such as dolomite and hollow spheres also diminish the strength of the casting, since the particles themselves act as sources of flaws.

5. Aspect ratio

The aspect ratio of the filler is defined as the ratio of the length to the diameter of the particles. For the type of particles discussed here it is difficult systematically to alter the aspect ratio, thus this part of the discussion will consider fibre reinforced materials since their fibre length may be relatively easily varied. The effect of aspect ratio on composite strength and toughness has been investigated by Kelly [10]. His results are shown in Fig. 7. The work of fracture increased with fibre length up to a critical size ℓ_c, thereafter the energy dropped. The strength, however, attained a maximum asymptotic value above ℓ_c (see Fig. 8) [12]. These results may be explained as follows: below ℓ_c the principal mechanism is fibre pull-out, whereas above ℓ_c fibre failure occurs. The maximum composite strength

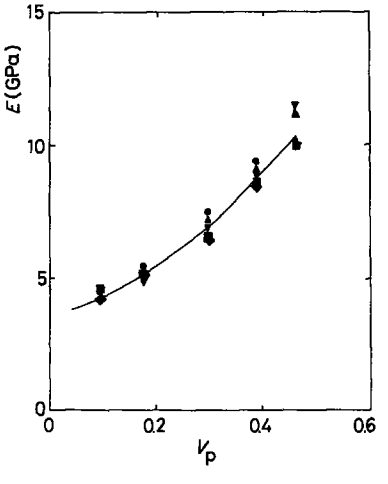

Figure 4 Variation in modulus, E, with volume fraction of filler for varying particle sizes. ●, 4.5 μm. ▲, 16 μm, ▼, 32 μm; ■, 47 μm; ◆, 62 μm (after Spandoukis and Young [7]).

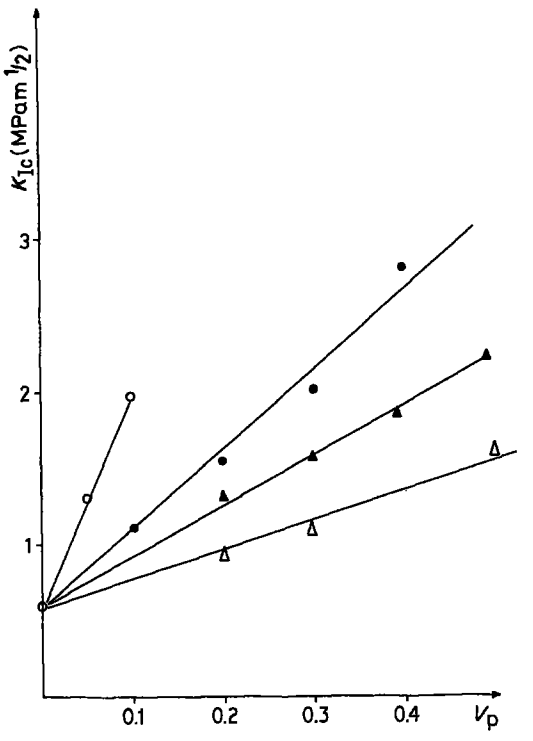

Figure 5 Stress intensity factor as a function of volume fraction of filler ▲, alumina and silica particles; △, A187 treated glass beads; ●, silicon carbide; ○, short glass fibres.

is obtained only when the full fibre strength may be utilized, i.e. above ℓ_c. Ideally to give optimal strength and toughness in every direction, fibres slightly longer than the critical length should be used in a three dimensional random array with a high volume fraction of fibres. This is extremely difficult to obtain in practice since most fabrication methods preferentially align fibres in a certain direction.

For particulate fillers, phenomena similar to those seen in fibres are observed. The data presented in Fig. 5 are for fillers of differing aspect ratio, the glass beads having an aspect ratio of 1, alumina and silica particles 2 to 3 and silicon carbide ~ 4, whereas that for the short glass fibres is ~ 15. It can be seen from these data that increasing filler aspect ratio increases the resistance to crack propagation, short glass fibres being the most effective. However, simple processing methods do not permit the incorporation of high volume fractions of short fibres due to the high viscosity of the uncured mixture.

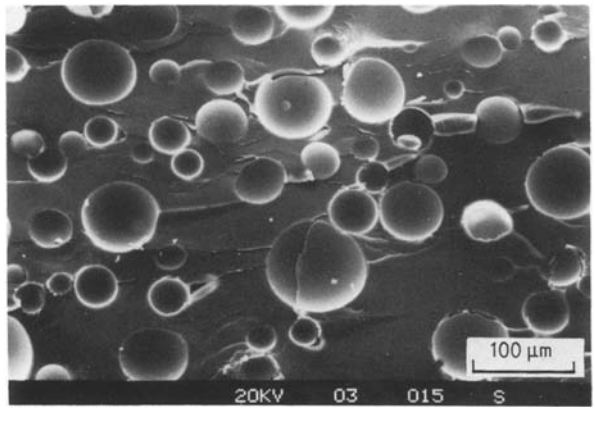

Figure 6 Fracture surface of a composite prepared from 30 vol % of hollow silica spheres in an epoxide matrix.

TABLE III Effect of surface treatment on strength and toughness

Resin	Filler	Treatment	Flexural strength (MPa)	Tensile strength (MPa)	K_c (MPa m$^{1/2}$)
A	Al_2O_3 30%	None	–	–	1.86
		HMDS	107	–	1.81
		A187	155	–	2.04
		A1100	145	–	1.99
B	Al_2O_3 30%	None	96	45	1.53
		HMDS	82	–	1.46
		A187	132	88	1.64
		A1100	136	–	1.67

TABLE IV The effect of surface treatment on the mechanical properties of glass bead composites (40 vol % beads, Type 2429 [13])

Resin	Treatment	Mean value K_c (MN m$^{-3/2}$)		Flexural strength
		Initiation	Arrest	
A	None	1.88	1.52	–
	CTMS	2.26	1.37	–
	A187	1.89	1.74	–
	A1100	1.96	1.73	–
B	None	1.57	1.35	59.8
	CTMS	1.75	1.21	–
	A187	1.45		69.8
	A1100	1.48		86.6

6. Resin–filler adhesion

In order to investigate the effect of altering the resin–filler adhesion on composite mechanical properties, both alumina and glass beads were used. The particles were treated with hexamethyldisilazane (HMDS) which would be expected to reduce the filler–resin adhesion and two commercial silane coupling agents γ-glycidoxypropyl trimethoxy silane A 187 and γ-aminopropyl triethoxysilane A 1100*. The micrographs of the fracture surfaces in Fig. 9 indicate that the adhesion was modified in the manner desired.

Spandoukis and Young [7, 8] who used glass beads treated with a mould release agent DC 1107 and the silane coupling agent A 187 found that surface treatment had little effect on the composite modulus (see Fig. 4). Similarly we have also observed that in the case of alumina particles the filler–resin adhesion does not change the toughness (see Table III). For two epoxide resins the K_c values for different filler surface treatments varied within the normal ~10% scatter. For glass bead filled systems, poorly bonded beads promoted crack tip blunting and unstable crack propagation (see Table IV) whereas stable propagation was found for well-bonded beads. Clearly different mechanisms intervene here and the K_c values do differ between surface treatments. These mechanisms will be discussed later.

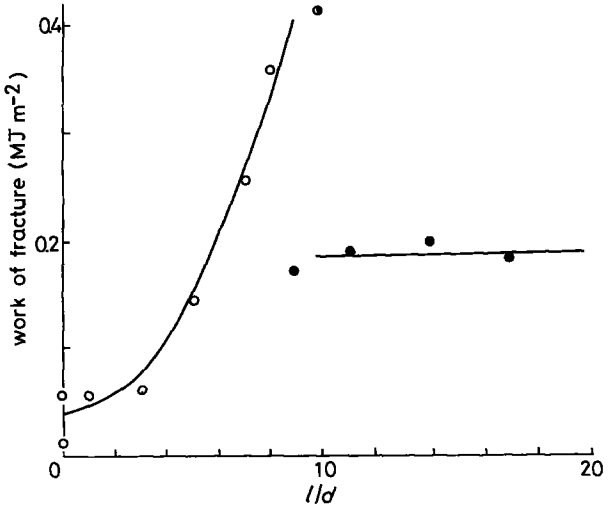

Figure 7 Variation of the work of fracture with the ratio of fibre length to fibre diameter (after Cooper and Kelly [11]). ○ pull-out, ◑ some pull-out, ● fibre failure.

Filler surface treatment does, however, have a significant influence on the strength of the castings. Well-bonded fillers give composites with notably higher flexural and tensile strength (Tables III and IV). This may be explained by weakly bonded particles acting as sources of "inherent" flaws provoking crack initiation. Effective inherent flaw sizes may be calculated from the following equation

$$K_{Ic} = \sigma Y a_i^{1/2}$$

where K_{Ic} is the critical stress intensity factor measured by, for example, the single edge notch test; σ is the tensile strength; Y is a geometric factor ($\pi^{1/2}$ for infinitely wide specimens, ~1.99 for single edge notched specimens), and a_i is the effective "inherent" flaw size. In unfilled epoxide resins, calculations of this kind give values of 15 to 50 μm and for filled resins 100 to 500 μm depending on the type of filler and the adhesion. The possible sources of these flaws will be discussed later.

It may be concluded that whereas poorly bonded glass beads give apparently higher toughness due to crack tip blunting, this is accompanied by a decrease in the strength of the composite and is therefore not beneficial for the overall performance.

7. Matrix toughness

The most successful means of improving the toughness of epoxide resins to date is by incorporation of a secondary dispersed phase of carboxyl terminated

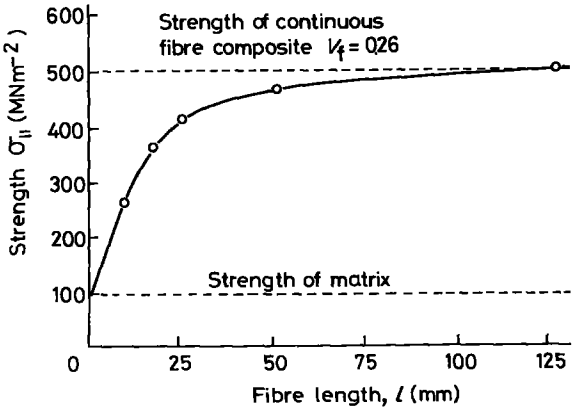

Figure 8 Tensile strength of fibres as a function of fibre length (after Hancock and Cuthbertson [12]).

*Trademark of Union Carbide.

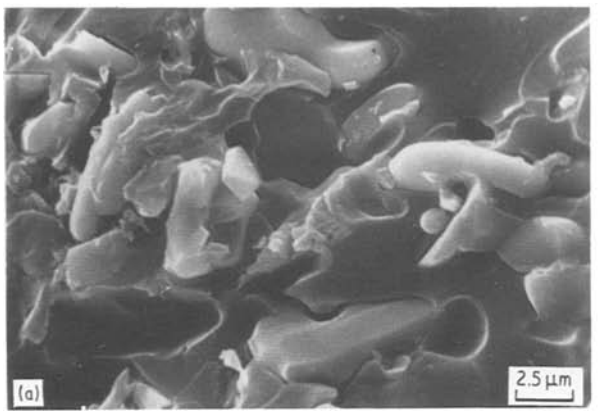

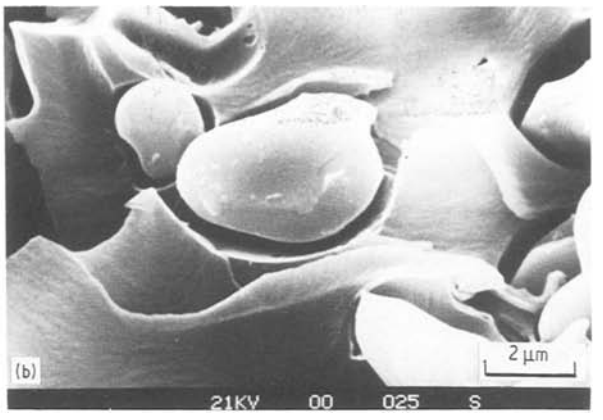

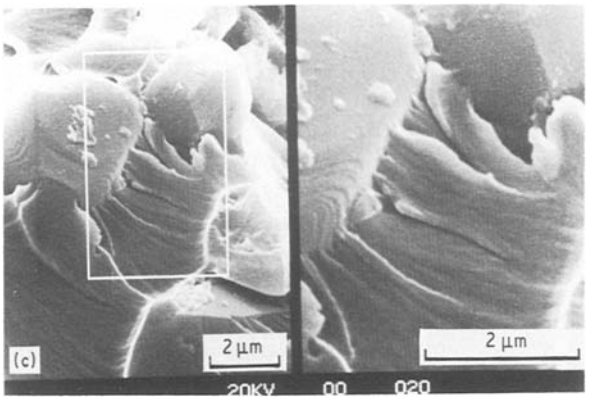

Figure 9 Fracture surfaces of alumina filled resin. (a) Untreated particles, (b) HMDS treated particles, (c) A 187 treated particles.

acrylonitrile butadiene rubber (CTBN). Much information on these systems is available in the literature [14]. Addition of CTBN at levels of 15 wt% gives four-fold increases in stress intensity factor (from $\sim 0.6\,MPa\,m^{1/2}$ to $\sim 2.5\,MPa\,m^{1/2}$) with only a small sacrifice in the modulus (decrease from ~ 3 GPa to ~ 2.7 GPa). Recently Maxwell and co-workers [15, 16] have reported results on hybrid systems containing epoxide resin, CTBN and glass beads. Instead of a linear relationship between K_c and volume fraction, a maximum in K_c was observed at $\sim 10\%$ glass. We have obtained similar results for a composite containing epoxide, CTBN and silica particles, as shown in Fig. 10. The mechanical properties of the formulation with a maximum in K_c is given in Table V and compared with the unmodified filled epoxide. It can be seen that the fracture energy is considerably increased without too great a loss in modulus or glass transition temperature however, the flexural and tensile strengths are somewhat impaired.

Pearson and Yee [17] have investigated the effect of changing the resin cross-link density on the toughness of CTBN modified epoxides. Their results are given in Table VI. Varying the epoxy equivalent weight between 172 and 2000 increased fracture energies (G_{Ic}) from 0.162 to $11.5\,kJ\,m^{-2}$. They concluded that intrinsic matrix ductility was the main source of toughness. Whether these high toughness systems could be used with particulate fillers to give hybrids with optimal toughness, moduli and strength remains to be seen. Unfortunately once again the high viscosity of these resins may well create problems and their lower glass transition temperature could limit applications.

The results of all these data are summarised for clarity in Table VII which gives the general trends in the composite strength, toughness and stiffness by varying properties of the two phases.

8. Direct observations of fracture in particulate filled epoxide resins

In order to investigate in further detail the mechanisms of fracture in two phase materials fracture tests have recently been conducted in the scanning electron microscope (SEM). The experimental arrangement has been described in [18]. The technique is potentially very powerful, however, certain problems are encountered: notably, in order to work at beam voltages above 1 kV it is necessary to coat the polymeric sample with a metallic layer such as gold or platinum in order to render the surface conductive. For the majority of the tests a layer of gold ~ 30 nm thick was applied. Unfortunately, the gold layer is incapable of following all the deformations of the polymer and the gold cracks during the fracture test. Thus, the plastic zone at the crack tip of the polymer appears to be full

TABLE V Mechanical properties of an unmodified filled and rubber modified filled epoxide resin

Formulation	Modulus (GPa)	Flexural strength (MPa)	Tensile strength (MPa)	K_c ($MPa\,m^{1/2}$)	G_c ($J\,m^{-2}$)	T_g (°C)
Epoxide 100 parts CTBN 15 parts Piperidine 5 parts Silica 90 parts	6.0	80	55	3.04	1540	96
Epoxide 100 parts Piperidine 5 parts Silica 90 parts	6.5	120	90	1.5	346	96

TABLE VI Fracture energy of unmodified and rubber modified epoxide resins of varying crosslink density (after Pearson and Yee [17])

Material	Epoxide equivalent weight (g)	G_{Ic} (kJ m^{-2})
Unmodified		
DER 332/DDS	172–176	0.162
DER 661/DDS	475–575	0.201
DER 667/DDS	1600–2000	0.326
Modified 10% CTBN		
DER 332/DDS/13 10%	172–176	0.223
DER 661/DDS/13 10%	475–575	2.41
DER 667/DDS/13 10%	1600–2000	11.5

TABLE VII Parameters determining the modulus, toughness and strength of particulate filled epoxide resins

Property	Effect on:		
	Modulus	K_c	Strength
Increase volume filler	Increase	Increase	~Constant at matrix value
Particle size	Constant	Constant	Decrease
Increase aspect ratio	–	Increase	Increase
Increase strength and modulus filler	Increase	Increase	Increase
Improved adhesion	Constant	Constant	Increase
Tougher matrix	Small decrease	Increase	Decrease

of fine "microcracks". This misled us in the early part of our experiments, and indeed two other groups of workers using the same technique on epoxides [19] and polyamides [20] have reported the same observation. It is now clear that these "microcracks" are only within the gold layer. In order to be able to differentiate between the artefacts caused by the gold coating and the real fracture characteristics, three approaches were used. Firstly, the gold coated specimens were fractured in the SEM which permitted the use of relatively high beam voltages (typically 10 kV) and hence good resolution. Secondly, samples without gold coating were fractured in a SEM equipped with an LaB_6 filament at very low beam voltages (1 kV). Thirdly, the same materials were fractured outside the microscope with and without gold coating, and both the deformed specimen and the fracture surfaces were observed under the optical microscope and SEM.

A further problem in investigating particulate filled resins by this technique is that being cast from liquid state the surface layer is resin-rich and thus must be removed to reveal the particles below. Many polishing techniques were attempted but the resin–particle interface was inevitably damaged, particles being torn out or broken. Study of micrographs of polished composites in the literature also showed evidence of surface damage during specimen preparation. Finally, the technique of argon ion etching was adopted. With careful control of current, voltage, time and angle of attack, satisfactory surfaces were obtained. An example is given in Fig. 11. Nevertheless the rubber modified resins were rather sensitive to the ion beam and etching time was kept to a minimum. In order to ensure that etching did not alter the surface layer additional experiments were carried out on polished and unetched specimens.

The specimen geometry used in these tests was the compact tension of size 14 × 13 × 2.5 mm. Samples were pre-cracked with a razor blade and then mounted in a specially designed testing jig which fitted onto the stage of a Cambridge Instruments scanning electron microscope S250. The specimen was loaded, and the crack propagation followed under the electron beam. The events were recorded by video but in some cases photographs were taken from the normal SEM raster which are of better quality. Photographs reproduced from the video are of poorer quality but certain events may only be captured by this means.

9. Mechanisms of fracture in unfilled and filled epoxide resins

9.1. Unmodified unfilled resins

Two types of crack propagation are observed in these systems either stable, continuous or unstable stick-slip propagation. The load–displacement curves for each type are shown in Fig. 12, and are relevant for test geometries where the compliance is linear with crack length (e.g. double torsion, tapered double cantilever

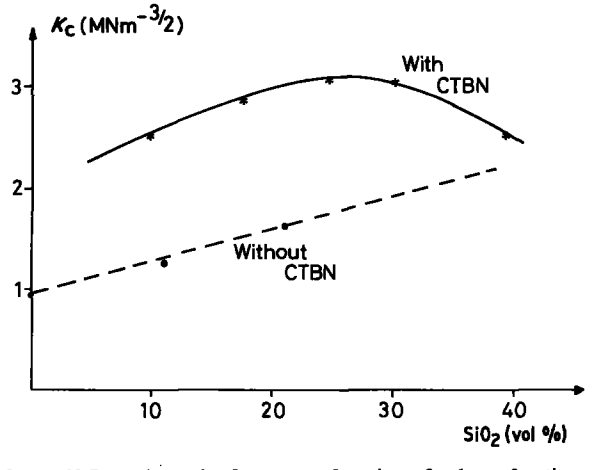

Figure 10 Stress intensity factor as a function of volume fraction of silica particles.

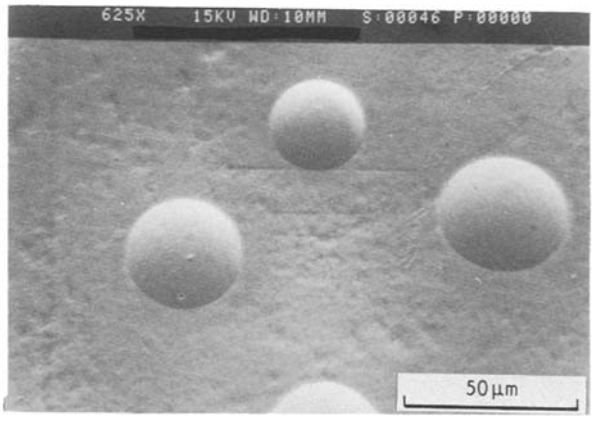

Figure 11 Surface of a glass bead filled resin after argon ion etching.

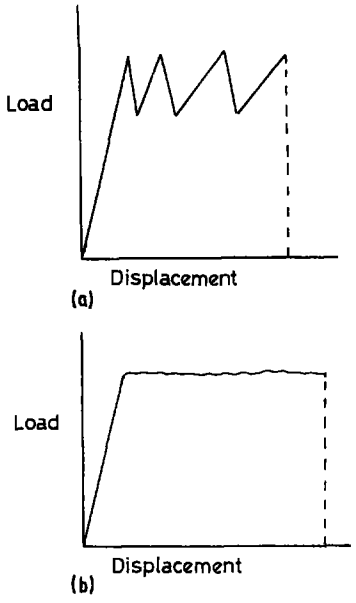

Figure 12 Typical load–displacement diagrams for (a) unstable and (b) stable crack propagation.

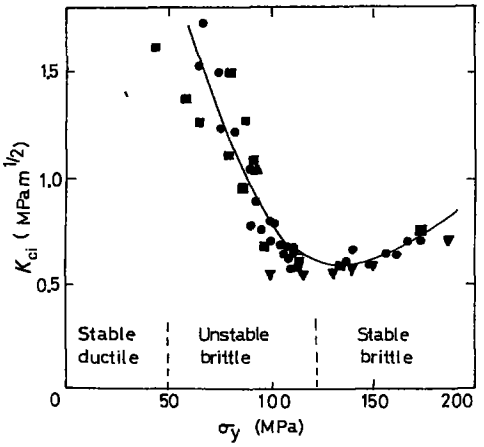

Figure 14 Plot of K_{ci} against the yield stress, σ_r, for different formulations of a DGEBA epoxy resin tested at a variety of rates and temperatures. The regions of different types of crack growth are indicated: ▼, 7.4 phr TETA; ●, 9.8 phr TETA; ▲, 12.3 phr TETA; ■, 14.7 phr TETA (after Yamini and Young [22]).

beam). The values of load may be used to calculate the stress intensity factor, K_c. For resins exhibiting stable crack propagation, K_c shows little rate dependence. (K_c and velocity ($\dot{a}$) are related by $K_c = B\dot{a}^n$. The value of n for unfilled resins is of the order of 90.) For a range of epoxides with differing chemical structure the values are situated in the range of 0.5 to 0.7 MPa m$^{1/2}$ at room temperature (see Table VIII). For resins exhibiting unstable crack propagation the load–displacement diagrams have a saw-tooth appearance, and values of K_c appropriate to crack initiation (K_{ci} and crack arrest (K_{ca}) may be determined (Fig. 12). Values of K_{ci} are, in general, strongly dependent on testing rate whereas K_{ca} values are approximately constant and similar to values for stable propagation. At higher testing speeds propagation often becomes continuous. An example of this behaviour is the resin Araldite B/HT 901 [21] (see Fig. 13).

Values of K_{ci} increase with decreasing testing speed; at 0.05 mm min^{-1} K_{ci} is 0.85 MPa m$^{1/2}$ whereas at higher speeds above 0.5 mm min^{-1} propagation is continuous and K_c is 0.65 MPa m$^{1/2}$. Yamini and Young [22] have explained the transition from stable to stick–slip crack propagation in terms of blunting at the crack tip. For resins with low yield stress material in the vicinity of the crack tip may flow whilst the crack is propagating causing crack tip blunting (see Fig. 14). A higher stress is required to re-initiate a sharp crack and hence the value of K_{ci} is greater than K_{ca}. The magnitude of K_{ci} is dependent on the radius of the blunted crack. Data for a range of epoxide resins may be fitted to this theory as shown by Kinloch and Williams [23].

The fracture tests conducted in the scanning electron microscope visualized directly this phenomenon of crack tip blunting. The process is shown in Figs 15 to 17 which were taken from the video recording. In Fig. 15 the crack tip is sharp, this is progressively blunted (Fig. 16) and in Fig. 17 a new sharp crack is initiated. In these micrographs the cracking of the gold layer is evident but the plastic zone is clearly delimited by this effect. Pronounced shear lips may be seen which derive from the shear deformations occurring at constant volume, hence the sample surface is sucked in. The plastic zone size may be readily measured from these experiments. For the resin shown in Fig. 18 the plastic zone is 40 μm in length and 15 μm in width.

The length of the plastic zone ahead of the crack tip may be calculated from the Dugdale model as follows:

$$R = \frac{\pi}{8}\left(\frac{K_c}{\sigma_p}\right)^2 \qquad (2)$$

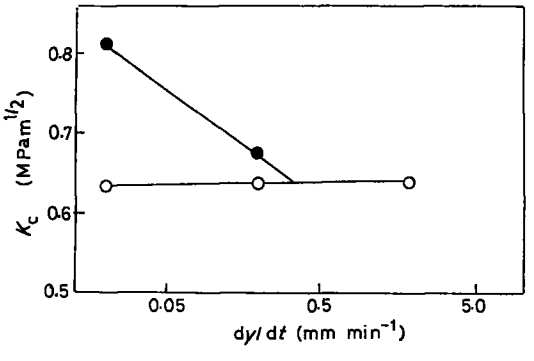

Figure 13 Variation in stress intensity factor with crosshead displacement rate for double torsion specimen of Araldite B/HT901 (after Yamini and Young [21]).

TABLE VIII Values of stress intensity factor for different epoxide resins showing stable crack propagation

Resin	K_c (MPa m$^{1/2}$)
Hydantoin resin/anhydride hardener	0.62
Cycloaliphatic resin/hexa hydro phthalic anhydride	0.56
Cycloaliphatic resin/methyl hexa hydropthalic anhydride	0.55
Cycloaliphatic resin/tetra hydro phthalic anhydride	0.74
Cycloaliphatic resin/methyl tetra hydro phthalic anhydride	0.54
DGEBPA resins/tetraethylene pentamine	0.5
DGEBPA resin/phthalic anhydride	0.45

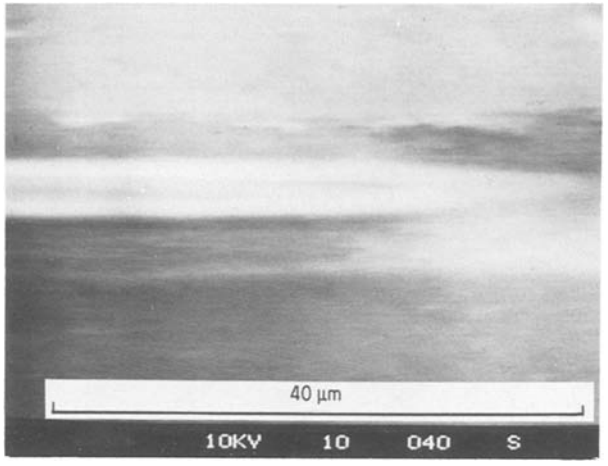

Figure 15 Sharp crack in an epoxide resin.

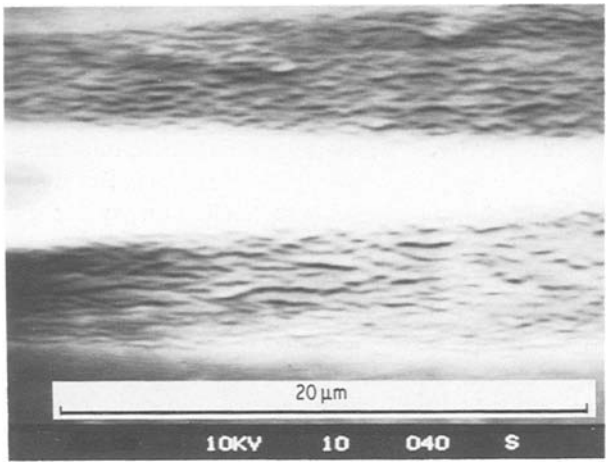

Figure 16 Original crack progressively blunts.

for plane stress conditions at the surface. Taking σ_p to be the yield stress of the resin (100 MPa) the value of R is 16.5 μm which is somewhat smaller than measured experimentally. The crack opening displacement (δ) may be calculated from:

$$\delta = \frac{K_c^2}{E\sigma_p} \quad (3)$$

where E is Young's modulus. The measured value of

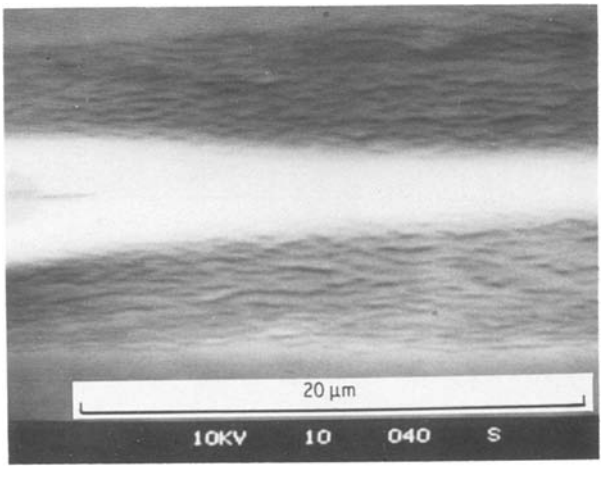

Figure 17 Initiation of a new sharp crack at the blunted tip (Figs 15–17] taken from video recording).

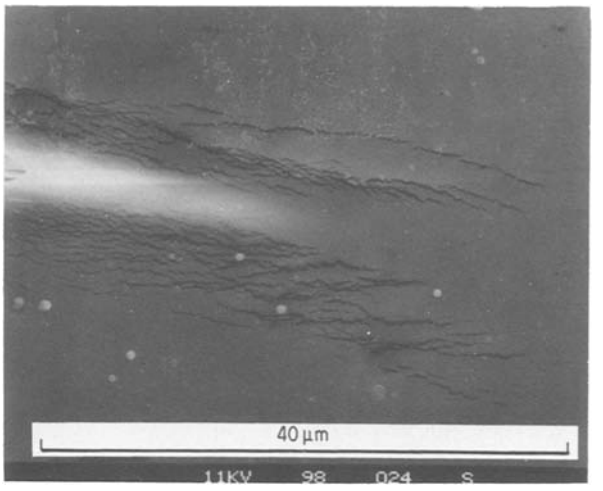

Figure 18 Crack tip zone in an unmodified unfilled epoxide resin.

2.4 μm is in reasonable agreement with the calculated value of 1.5 μm.

There is an increasing amount of evidence in the literature which indicates that the primary mode of deformation in epoxides is by shear yielding both in unmodified resins, rubber modified systems [24, 25] and in composite materials with epoxide matrices [26]. There have been some reports of crazes in epoxides but for particular cases such as when straining very thin films [27] or for resins with extremely low cross-link density [28] which thus approach thermoplastic behaviour.

9.2. Particulate filled resins

Incorporation of particulate fillers into epoxide resins tends to stabilize fracture. The resin Araldite B/HT901 which exhibited unstable crack propagation when unfilled, showed stable propagation with filler levels of above 20 vol % silica or alumina. For these stable systems the increase in toughness over the unfilled resin is consistent with the mechanism of crack pinning, shown schematically in Fig. 19. This mechanism was originally suggested by Lange [29] and is analogous to the line tension concept used in dislocation theory. The concept was analysed further by Evans [30] who calculated the increase in energy required to bow the crack in terms of the ratio of the particle size to the particle spacing (r/c). The values were recalculated by Green and co-workers [31] who

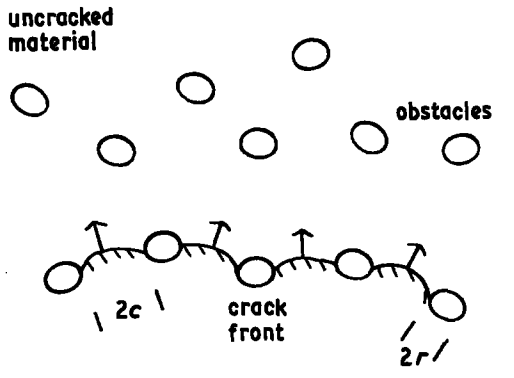

Figure 19 Schematic representation of the process of crack pinning.

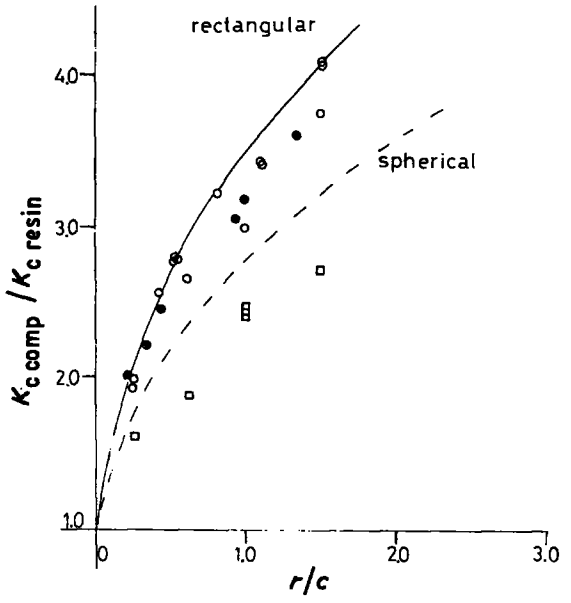

Figure 20 The increase in stress intensity factor required to move a crack through a series of obstacles: ——, theoretical curve for rectangular obstacles; – – –, theoretical curve for spherical obstacles; ○, silica particles; ●, alumina particles; □, glass beads treated with A187.

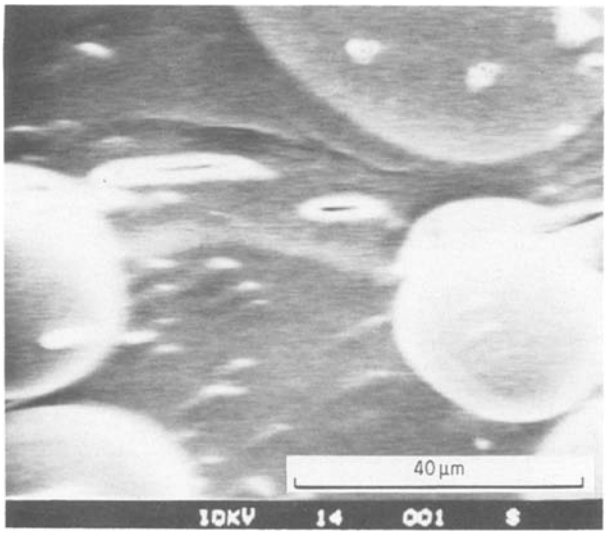

Figure 21 Void initiation ahead of the crack tip in a composite prepared from silane treated glass beads.

give the increase in stress intensity factor for spherical and rectangular particles. The theoretical curves are shown in Fig. 20 and compared to the experimental data for silica, alumina and silane treated glass beads. Silica and alumina particles approximate quite well to rectangular inclusions, whereas glass bead composites have lower values than theoretically predicted for spherical inclusions. Kinloch *et al.* [32] have recently observed strained thin films of glass bead filled epoxides by optical interference microscopy and obtained direct evidence of crack bowing between particles.

The fracture experiments in the SEM on glass bead filled resins gave no evidence of crack pinning, rather voids were initiated ahead of the crack tip. In the case of well-bonded glass beads these voids were nucleated within the matrix some 1 to 3 μm away from the resin–filler interface as shown in Fig. 21. For poorly bonded beads crack propagation was highly unstable and too rapid to follow under the electron beam at high magnifications. In these systems decohesion occurred at the interface ahead of the crack tip. This phenomenon has also been reported by Owen [33] and Su and Suh [34]. It appears that this debonding of the particles gives rise to crack tip blunting and unstable propagation. Thus, for the glass bead systems with weakly bonded particles there may be competition between pinning and blunting.

It is clear from the preceding discussion that the aspect ratio is an important parameter in determining fracture mechanisms. For particles with much higher aspect ratios, like short glass fibres, other energy consuming mechanisms intervene such as fibre pull-out and fibre deformation and fracture. Faber and Evans [35] have proposed that in such systems crack deflection is important, shown schematically in Fig. 22. However, the fracture surface of the resins filled with short glass fibres are much more consistent with fibre pull-out than crack deflection (see Fig. 23).

9.3. Rubber modified resins

The fracture behaviour of rubber modified epoxide resins has been studied in some detail in recent years. Considerable increases in fracture energy are observed

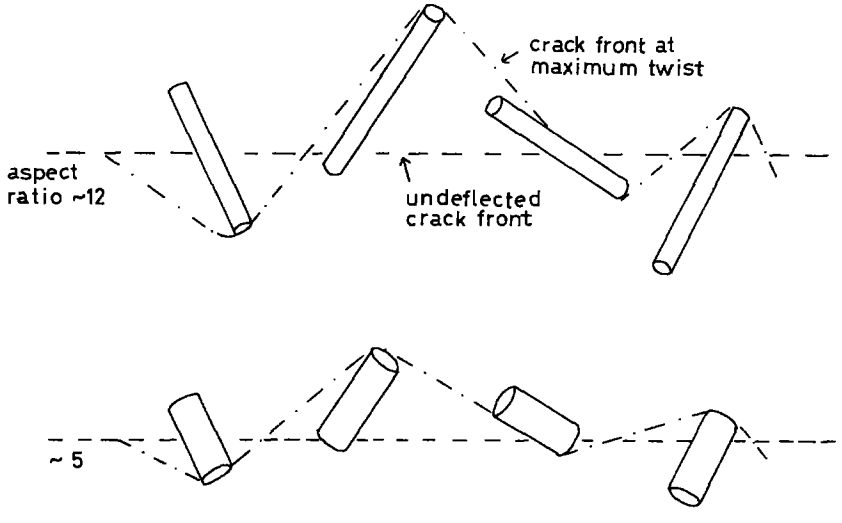

Figure 22 Schematic diagram of twist of a crack around rods of two aspect ratios, R, at constant volume fraction (after Faber and Evans [35]).

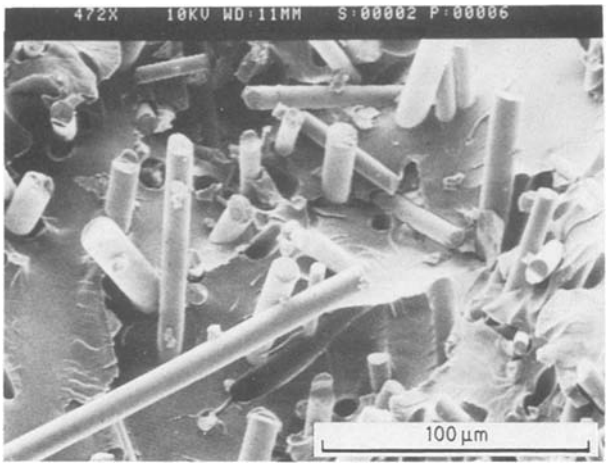

Figure 23 Fracture surface of a resin filled with short glass fibres.

which may be up to sixty fold for some systems. A number of different mechanisms have been proposed such as deformation of the rubber particles across the crack tip [36], crazing of the matrix [37] or absorption of energy by the matrix [38]. There is now, however, considerable evidence in the literature [24, 25] that the high toughness derives from blunting of the crack produced by cavitation of the rubber particles under the triaxial stress state at the crack tip. This cavitation lowers the local yield stress and provokes extensive shear yielding. The fracture surface of these rubber modified resins is covered with holes as shown in Fig. 24. The rubber in fact forms a lining in these depressions. The plastic zone sizes and crack opening displacements (COD's) are considerably higher than for the unmodified resins. From the fracture tests in the SEM, COD's were measured to be $\sim 10\,\mu m$ and plastic zone sizes some hundreds of microns. The crack tip zone for a rubber modified resin is shown in Fig. 25 which is for a sample cracked without gold coating and observed at low voltage. The furrows derive from the shear deformation ahead of the crack. Comparison with Fig. 18 indicates the much larger plastic zone size in the modified systems.

Some isolated cases of material bridging the crack were observed (see e.g. Fig. 26a). However, this is probably epoxide rather than rubber since after fracture the broken moieties do not retract as would be characteristic of rubber (Fig. 26b) and their size is some $40\,\mu m$, that is considerably larger than the rubber particles which are ~ 1 to $5\,\mu m$. Moreover, if the rubber deformation model [36] were correct a forest of deformed rubber particles would be observed at the crack tip.

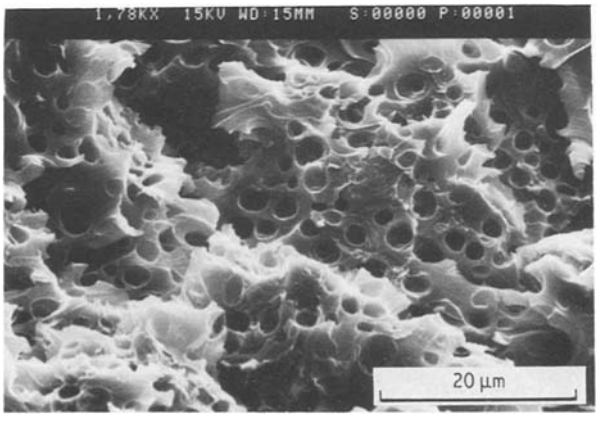

Figure 24 Fracture surface of a rubber modified epoxide resin. The "stress whitened" surface results from deformation and cavitation of the rubber particles which appear here as holes.

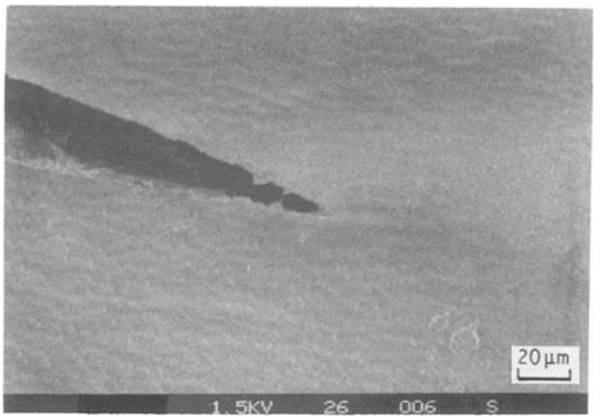

Figure 25 Crack tip zone of a rubber modified epoxide under load in the SEM. The sample was not coated with gold and observed at 1.5 kV.

9.4. Rubber modified filled resins (hybrids)

A typical fracture surface of a hybrid resin is shown in Fig. 27. The holes resulting from the cavitated rubber particles are once again evident and the glass beads, having been silane treated, are well bonded to the matrix. Some beads are fractured as shown in the left of Fig. 27, particularly those with voids.

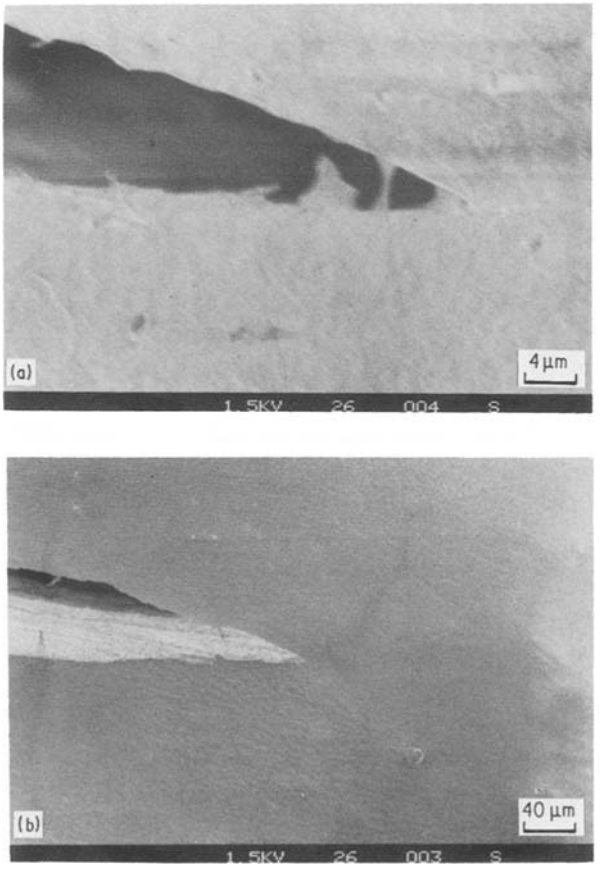

Figure 26 (a and b) Crack tip zone in a rubber modified epoxide under load in the SEM (conditions as in Fig. 25).

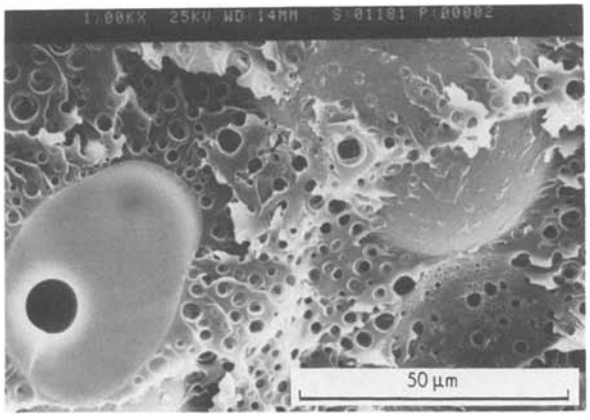

Figure 27 Fracture surface of a hybrid resin (epoxide + CTBN + silane treated glass beads).

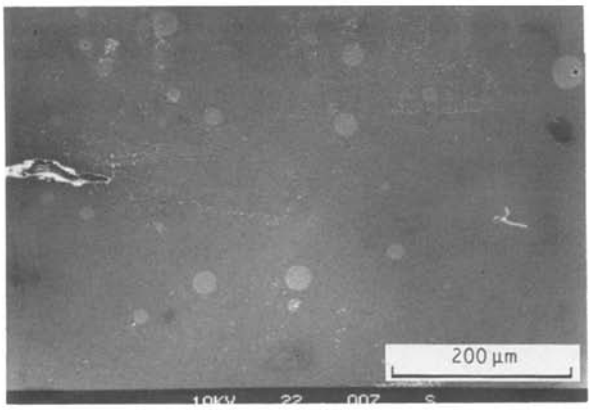

Figure 28 Fracture of a hybrid epoxide resin.

The mechanisms of fracture of these hybrids are still unclear. The fracture tests conducted in the SEM showed a highly discontinuous fracture. A crack propagated a certain distance, blunted and stopped. Rather than this crack continuing, a new void was initiated some tens to hundreds of microns from the original crack tip. In this manner the type of crack propagation observed in the rubber modified unfilled system and the particulate filled resin was superimposed. The plastic zone sizes and crack opening displacements were of the same order of magnitude as the rubber modified resins.

Certain evidence points to the conclusion that in the hybrid systems the shear deformations in the rubber modified matrix are altered by the presence of inorganic filler. Fig. 28 shows an image taken from the *in situ* fracture tests. Once again the gold layer cracked but around the glass beads the deformations are clearly different from those observed in the matrix.

10. Strength of particulate filled resins in the short and long term

10.1. Sources of flaws

As mentioned in Section 6, calculations of effective "inherent" flaw sizes give values in the range of 15 to 500 μm depending on filler content, size, type etc. The data for a number of systems have been collected in Table IX. In order to optimize the strength of filled resins it is necessary to understand the origin of these flaws. Various possibilities are listed below.

10.1.1. Specimen preparation

Defects initiating fracture may arise during specimen preparation such as air bubbles [39], resin-rich areas (see Fig. 29), or foreign matter (see Fig. 30) such as dust particles [40]. It is clear that precautions during sample manufacture can eliminate this type of flaw.

10.1.2. Particle size

The flaw sizes found for silica filled composites are of the order of 100 μm which may be explained by the presence of particles significantly larger than the mean size which, in this case, is 50 μm. Particles of size 80 to 100 μm may indeed be found on the fracture surfaces (see Fig. 31).

10.1.3. Poorly bonded or weak particles

The large flaw sizes found for untreated alumina filled composites (290 μm) probably derive from the linking up of weakly bonded particles. An example of this type may be seen in Fig. 32. The flaw sizes of composites prepared from alumina trihydrate were in the range 300 to 500 μm. These particles are relatively

TABLE IX Calculated "inherent" flaw sizes for a range of filled epoxide resins

Filler	Mean particle size (μm)	Volume fraction (%)	Tensile strength (MPa)	K_c (MPa m$^{1/2}$)	Flaw size (μm)
–	–	–	78	0.47	13
Silica	50	20	47	0.99	132
Silica	50	40	64	1.49	96
Silica	50	50	78	1.65	115
Alumina (untreated)	6	30	45	1.53	290
Alumina (silane treated)	6	30	88	1.64	87
–	–	–	76	0.91	36
Alumina trihydrate*	5	29.5	33	1.34	412
Alumina trihydrate	8	10	30	1.22	413
Alumina trihydrate	8	21.5	34	1.51	493
Alumina trihydrate	8	29.5	45	1.51	282
Alumina trihydrate	8	43	38	1.44	359
Alumina trihydrate	12	29.5	35	1.60	522

*Data from [41].

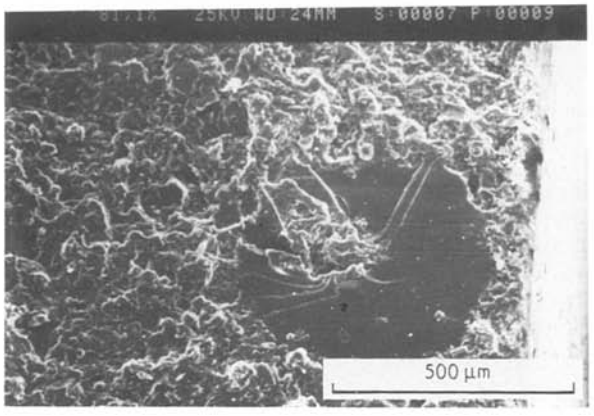

Figure 29 Fractured tensile specimen of silica filled epoxide resin showing rupture initiated within a resin-rich area.

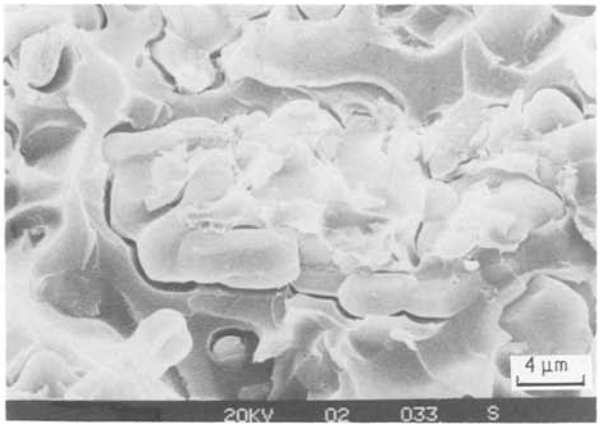

Figure 32 The fracture surface of an alumina filled resin showing how poorly bonded particles may link up to create larger flaws.

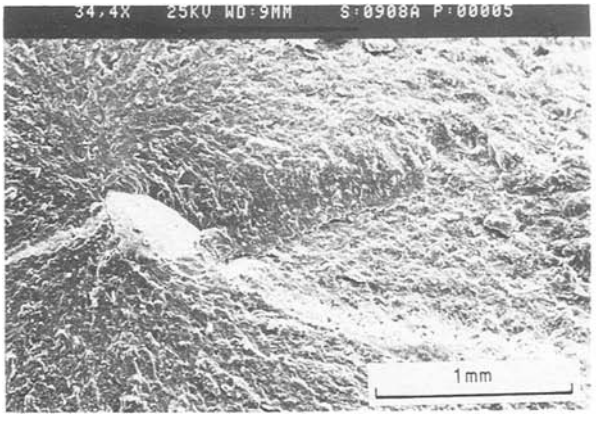

Figure 30 Fractured tensile specimen of silica filled epoxide resin showing rupture initiated at a foreign body incorporated inadvertantly into the casting during specimen preparation.

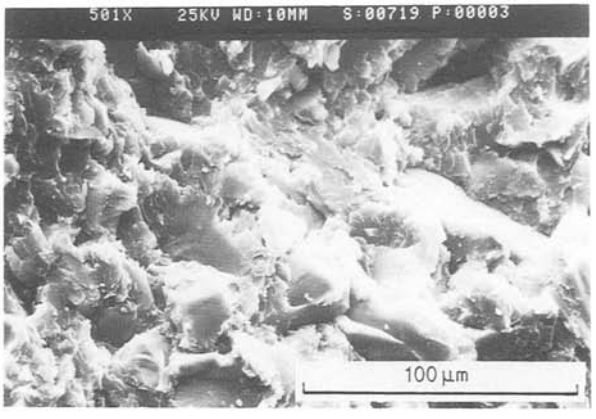

Figure 33 Fracture surface of a tensile specimen of silica filled epoxide resin tested at RT (fracture time ~ 10 min).

weak and fractured particles are frequently found on the ruptured surface. Thus, in this case, flaws probably derive from a series of particles broken during the test.

10.1.4. Flaws generated during testing

Treatment of alumina particles with a silane coupling agent increased significantly the tensile strength and hence reduced the flaw size from 290 to 87 μm. These alumina particles are in the size range 4 to 6 μm and therefore, unlike silica, cannot derive from particles of above average size. In this case it appears that flaws develop during the test perhaps by the coalescence of microvoids or by the plastic deformation of a certain zone of the sample. The initiation of defects is difficult to study experimentally but definitely merits further investigation.

10.2. Static fatigue

The lifetimes of a number of filled epoxide resins under constant load may be predicted on the basis of the relationship between the stress intensity factor and the crack velocity [42, 43]. Good agreement has been obtained between calculated lifetimes and measurements up to times of two years for temperatures up to

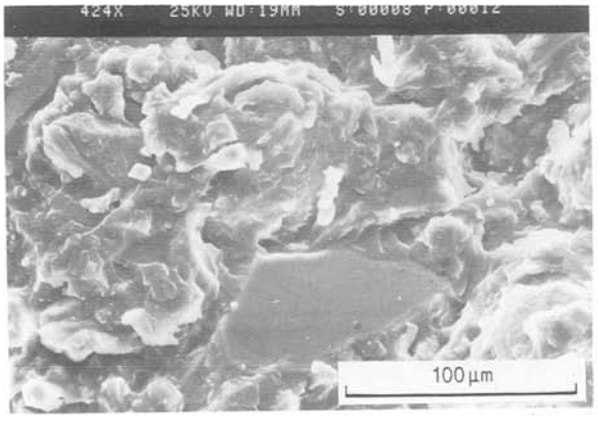

Figure 31 Fracture surface of a silica filled epoxide resin showing particles of size approaching the calculated "inherent flaw" size.

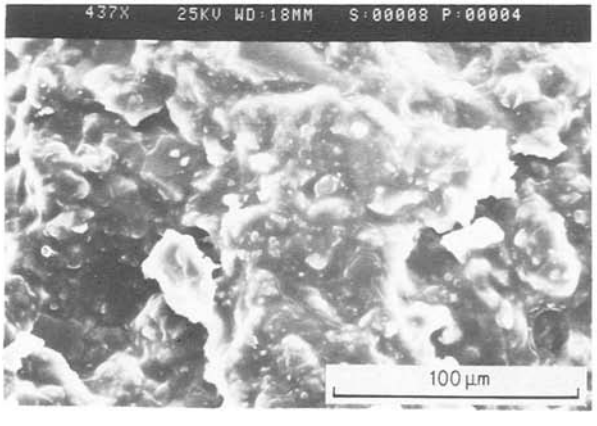

Figure 34 Fracture surface of a tensile specimen of silica filled resin maintained at 70% ultimate/85° C (i.e. 35° C below T_g).

about 20° C below the glass transition temperature [44]. The analysis assumes that the long term fracture mechanism is sub-critical crack growth from pre-existing flaws. However, there is little direct evidence that this is the correct mechanism. Microscopic evidence indicates that different mechanisms operate in short and long term. In particular the combination of sustained loads and elevated temperatures produce fracture surfaces with features dissimilar from those resulting from a tensile test at room temperature (Figs 33 and 34). The study of this phenomenon forms part of a continuing research programme to predict and improve the lifetime of filled thermosetting polymers.

References

1. L. J. BROUTMAN and S. SAHU, *Mater. Eng. Sci.* **8** (1971) 98.
2. S. J. FELTHAM, B. YATES and R. J. MARTIN, *J. Mater. Sci.* **17** (1982) 2309.
3. M. NARKIS, *J. Appl. Polym. Sci.* **22** (1978) 2391.
4. J. A. MANSON and L. H. SPERLING, in "Polymer Blends and Composites" (Plenum, New York, 1976) Ch. 12.
5. O. ISHAI and L. J. COHEN, *Int. J. Mech. Sci.* **9** (1967) 539.
6. A. C. MOLONEY, H. H. KAUSCH and H. R. STIEGER, *J. Mater. Sci.* **18** (1983) 208.
7. J. SPANDOUKIS and R. J. YOUNG, *ibid.* **19** (1984) 487.
8. *Idem., ibid.* **19** (1984) 473.
9. P. S. THEOCARIS, *Fibre Sci. Technol.* **19** (1983) 157.
10. A. KELLY, *Proc. Roy. Soc. Lond.* **A319** (1970) 95.
11. G. A. COOPER, and A. KELLY, in Proceedings of the International Conference on Mechanics Composite Materials, edited by F. W. Wendt (Pergamon, 1967).
12. P. HANCOCK and R. C. CUTHERTSON, *J. Mater. Sci.* **5** (1970) 762.
13. A. C. MOLONEY, H. H. KAUSCH and H. R. STIEGER, *ibid.* **19** (1984) 1125.
14. A. J. KINLOCH and R. J. YOUNG, "Fracture Behaviour of Polymers" (Applied Science Publishers, London, 1983) Ch. 11.
15. D. L. MAXWELL, R. J. YOUNG and A. J. KINLOCH, *J. Mater. Sci. Lett.* **3** (1984) 9.
16. A. J. KINLOCH, D. L. MAXWELL and R. J. YOUNG, *J. Mater. Sci. Lett.* **4** (1985) 1276.
17. R. A. PEARSON and A. F. YEE, *Polym. Mater. Sci. Eng.* **49** (1983) 316.
18. A. C. MOLONEY and H. H. KAUSCH, *J. Mater. Sci. Lett.* **4** (1985) 289.
19. S. BANDYOPADHYAY, V. M. SILVA, H. WROBEL and J. NICHOLLS, in Proceedings of the 6th International Conference Def. Yield & Fracture of Polymers, Plastics and Rubber Institute, Cambridge, April 1985.
20. N. SATO, T. KURAUCHI, S. SATO and O. KAMIGAITO, *J. Mater. Sci.* **21** (1986) 1005.
21. S. YAMINI and R. J. YOUNG, *Polymer* **18** (1977) 1075.
22. *Idem, J. Mater. Sci.* **15** (1980) 1823.
23. A. J. KINLOCH and J. G. WILLIAMS, *ibid.* **15** (1980) 987.
24. A. F. YEE and R. A. PEARSON, "Toughening mechanisms in elastomer modified epoxy resins", Part I., (NASA Report 3718, 1983).
25. A. J. KINLOCH, S. J. SHAW, D. A. TOD and D. L. HUNSTON, *Polymer* **24** (1983) 1341.
26. W. D. BASCOM, D. J. BOLL, D. J. FULLER and P. J. PHILLIPS, *J. Mater. Sci.* **20** (1985) 3184.
27. R. J. MORGAN and J. E. O'NEAL, *ibid.* **12** (1977) 1966.
28. A. VAN DEN BOOGAART, "Physical Basis of Yield in Glassy Polymers", edited by R. N. Haward (Institute of Physics, London, 1966).
29. F. F. LANGE, *Phil. Mag.* **22/179** (1970) 983.
30. A. G. EVANS, *ibid.* **26** (1972) 1327.
31. D. J. GREEN, P. S. NICHOLSON and J. D. EMBERY, *J. Mater. Sci.* **14** (1979) 1657.
32. A. J. KINLOCH, D. L. MAXWELL and R. J. YOUNG, *ibid.* **20** (1985) 4169.
33. A. B. OWEN, *ibid.* **14** (1979) 2523.
34. K. B. SU and N. P. SUH, *Soc. Plastics Eng.* **27** (1981) 46.
35. K. T. FABER and A. G. EVANS, *Acta Metall.* **31**(4) (1983) 565.
36. S. KUNZ-DOUGLAS, P. W. R. BEAUMONT and M. F. ASHBY, *J. Mater. Sci.* **15** (1980) 1109.
37. C. B. BUCKNALL, *Adv. Polym. Sci.* **27** (1978) 121.
38. J. N. SULTAN, R. C. LAIBLE and F. J. MCGARRY, *Appl. Polym. Symp.* **16** (1971) 127.
39. K. C. RADFORD, *J. Mater. Sci.* **6** (1971) 1286.
40. R. P. KAMBOUR and E. A. FARRAYE, in Proceedings of the 6th International Conference Def. Yield Fract. of Polymers, Cambridge, April 1985.
41. F. F. LANGE and K. C. RADFORD, *J. Mater. Sci.* **6** (1971) 1197.
42. R. J. YOUNG and P. W. R. BEAUMONT, *ibid.* **10** (1975) 1343.
43. B. J. PLETKA and S. M. WIEDERHORN, *ibid.* **17** (1982) 1247.
44. H. R. BEER, T. KAISER, A. C. MOLONEY and H. H. KAUSCH, *ibid.* **21** (1986) 3661.

Received 13 January
and accepted 30 June 1986